230 | https://doi.org/10.3311/PPtr.18453
Creative Commons Attribution

Periodica Polytechnica Transportation Engineering, 51(3), pp. 230–241, 2023

Calibration Measurements and Computational Models of Sensors Used in Autonomous Vehicles

Csaba Hajdu[1*], István Lakatos[2**]

[1] Department of Informatics, Széchenyi István University, Egyetem tér 1., H-9026 Győr, Hungary
[2] Department of Road and Rail Vehicles, Audi Hungaria Faculty of Automotive Engineering, Széchenyi István University, Egyetem tér 1., H-9026 Győr, Hungary
* Corresponding author, e-mail: hajdu.csaba@ga.sze.hu
**Corresponding author, e-mail: lakatos@sze.hu

Received: 29 April 2021, Accepted: 05 April 2023, Published online: 03 May 2023

Abstract

An increasing number of vehicles are equipped with cameras. As perception sensors, they scan the surrounding area and supply the Advanced Driver Assistance Systems (ADAS) for building up an environmental model through the use of computer vision techniques. While they perform well under good weather conditions their efficiency is reduced by adverse environmental influences such as rain, fog and occlusion through dirt. As a consequence, the vision based ADAS obtains poor quality information, and the model also becomes faulty. This paper deals with methods to estimate information quality of cameras in order to warn the assistance system of possible wrong working conditions. In particular, situations of contamination or occlusion of the windshield or camera lens, as well as foggy weather are taken into account in this paper. In the issue of occlusion total, fractional and transparent effectuations have to be recognized and distinguished. Therefore, this paper proposes an approach based on edge analysis of consecutive frames and presents initial experimental results of the implementation. In the field of Fog Detection a method based on the Logarithmic Image Processing Model is described and the results are shown.

Keywords

ADAS, sensor, radar, camera, calibration

1 Introduction

Nowadays, electronic equipment of vehicles is becoming more complex and increasingly important. Recent vehicles are equipped with numerous cameras and radar sensors to assist driver assistance systems and other safety and comfort functions. Furthermore, with the emergence of autonomous vehicles, intelligent functions require proper and precise sensory input. Proper installation and verification of sensor systems are therefore mandatory in current vehicles.

In this article, a new automotive laboratory capable of carrying out sensor calibration processes is presented. The laboratory is under construction and shall be able to calibrate both conventional vehicles and autonomous vehicles. This laboratory shall be equipped with the proper equipment for precise camera and radar calibration. Before describing the laboratory and its equipment, the technical background of sensor models is discussed, as calibration methods can perform tasks on camera and radar sensors. Additionally, LiDAR sensors are discussed, as they have a prominent presence on autonomous vehicles for localization and object detection tasks.

In the discussion of calibration algorithms, we differentiate between extrinsic and intrinsic calibration. Intrinsic calibration is sensor-specific, sometimes performed by the sensor manufacturers themselves. In some cases, it is performed mechanically and is well-researched area (e.g., cameras). On the other hand, extrinsic calibration estimates the kinematic transformation between multiple sensors. The process is formalized as an optimization process. Therefore, numerous methods can be employed for precise results. Estimating the kinematic structure of sensors is mandatory for intelligent algorithms to operate correctly (e.g., estimating the position of an obstacle). In this regard, this article reviews recent research performed in the extrinsic calibration of multiple sensors. This research also provides a way to setup a calibration plate for joint LiDAR, camera, and radar calibration.

Cite this article as: Hajdu C., Lakatos, I. (2023) "Calibration Measurements and Computational Models of Sensors Used in Autonomous Vehicles", Periodica Polytechnica Transportation Engineering, 51(3), pp. 230–241. https://doi.org/10.3311/PPtr.18453

The proposed laboratory can perform camera and radar calibrations, suitable for routine sensor calibration of conventional vehicles of numerous types (e.g., ones equipped with 360° sensor systems). Additionally, this laboratory could be used to perform extrinsic calibration for autonomous vehicles. In the laboratory introduction section, the steps to setup and perform the calibration is depicted in detail.

2 Sensor models

2.1 Overview of sensor models

This article discusses various approaches to exteroceptive automotive sensors (i.e., which perceive the surrounding environment of the vehicle) and a proposed real-world use-case. Very closely related to the calibration algorithms, Section 2.1 primarily discusses the computational models of popular sensors. As the calibration identifies features detectable by these sensors, calibration processes depend indirectly on the mathematical model of the sensors. In this article, mathematical models of the following sensors are further discussed, which are currently popular in autonomous vehicle applications:

- (Monocular) camera and stereo cameras: used to capture color video data. Cameras have relatively fast update frequency (even up to around 300 frames per second) but at a limited measurement range compared to LiDARs and radars. Additionally, camera usage is problematic in limited light conditions (e.g., tunnels, nighttime).
- Light Detection and Ranging (LiDAR): used for precise distance information measurement, in the form of a point cloud data. LiDARs can measure in a relatively large range and are not obscured by light conditions. On the other hand, their update frequency is relatively slow compared to RADARs and cameras.
- RADAR: used to measure the distance of objects in a conical field range. This sensor can achieve a fast update rate. Additionally, RADARs can also measure the velocity of detected objects.

Sensors are typically connected via some sort of serial (e.g., USB, UART) or network connection (predominantly Ethernet). In the case of cameras, it is also possible to use a dedicated embedded physical interface (e.g., MIPI-CSI 2 compatible) for camera feed. Automotive-certified sensors often offer the possibility to be powered from an external source. An important task is the precise time synchronization between the endpoints for time-synchronized data acquisition. Many network-connected sensors provide the use of modern time synchronization protocols (e.g., IEEE 1588-2019, 2019).

2.2 LiDAR

LiDAR (light detection and ranging) measures distance information by emitting laser beams from a vertical block of lasers. The number of the vertical beams also defines the channel number of the sensor (i.e., the number of measurable co-centric planes). The primary tasks of LiDARs in automotive systems are localization (e.g., by fusing additional IMU, RADAR, GPS sensors), obstacle detection, and ground segmentation. Also, mapping methods (SLAM) and some segmentation methods (like PointNet) utilize the LiDAR point cloud as input. Typical LiDARs are the Ouster OS-1 models and the Velodyne sensors. Some popular LiDARs and their respective properties are summarized in Table 1. Due to their extensive use in localization tasks, some sensors combine other sensors. A prominent example is the Ouster LiDARs which are combined with an inertial measurement unit (IMU).

LiDARs output a point cloud of distance information and intensity. The distance of a single point can be calculated simply by the light reflection formulae (similarly in the case of Sonar and RADAR technologies):

$$d = \frac{t_e \cdot c}{2}, \tag{1}$$

where t_e is the emission time of the beam, c is the speed of light ($c \approx 3 \cdot 10^8$ m/s). Based on the models defined in

Table 1 Summary of popular LiDARs

Name	Producer	Operation method	(FoV)°	Range (m)	Channels
OS1-32	Ouster	Digital spinning	45° (± 22.5°)	120 m	32
OS1-64	Ouster	Digital spinning	45° (± 22.5°)	120 m	64
OS1-128	Ouster	Digital spinning	45° (± 22.5°)	120 m	128
OS2-128	Ouster	Digital spinning	22.5° (± 11.25°)	240 m	128
VLP-16	Velodyne	Analog spinning	30° (± 15°)	100 m	16
HDL-32E	Velodyne	Analog spinning	40° (−30°, 10°)	100 m	32
HDL-64E	Velodyne	Analog spinning	26.9° (−24.9°, 2°)	120 m	64
2020	Pioneer	Raster	Variable	170 m	76 × 76

technical literature, the following sensor model can be defined (summarized in Fig. 1). The parameters associated with this model are the following:

- The step number of the side-block (n_e) and the steps required for one revolution n_{max}. For example, in the case of OS-1, this value is set to 90112.
- Range r from the data block is typically defined in millimeters (mm). Most sensors can achieve this precision.
- The elevation angle of one laser beam (ε_a).
- The side angle of a beam derived from internal parameters (α_a).

A point in the right-handed XYZ Cartesian coordinate is measured with the following formulae (based on cylindrical mapping):

$$\theta = 2\pi\left(\frac{n_e}{n_{max}} + \frac{\alpha[i]}{360}\right),\ \ \phi = 2\pi\left(\frac{\epsilon[i]}{360}\right), \tag{2}$$

$$x = r\cos\theta\cos\theta,\ \ y = -r\sin\theta\cos\theta,\ \ z = r\sin\phi. \tag{3}$$

This mapping can be rewritten in a Matrix-based formalism to define the forward sensor model and to derive the inverse sensor model. Given x, y, z coordinates the forward sensor model derives the range, side- and elevation angle:

$$\begin{bmatrix} r \\ \alpha \\ \varepsilon \end{bmatrix} = \boldsymbol{h}(x,y,z) = \begin{bmatrix} \sqrt{x^2+y^2+z^2} \\ \tan^{-1}\left(\frac{y}{x}\right) \\ \sin^{-1}\left(\frac{z}{\sqrt{x^2+y^2+z^2}}\right) \end{bmatrix}. \tag{4}$$

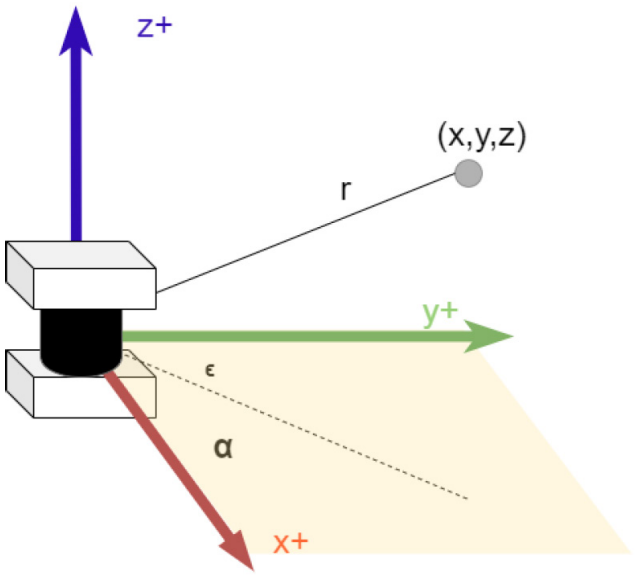

Fig. 1 Graphical representation of LiDAR sensor model

LiDARs measure with some degree of noise. In general, it is modeled as an additive noise following normal Gaussian distribution. In the case of the forward sensor model (v follows normal distribution $v \sim N(0, R)$):

$$\begin{bmatrix} r \\ \alpha \\ \varepsilon \end{bmatrix} = \boldsymbol{h}(x,y,z,v) = \begin{bmatrix} \sqrt{x^2+y^2+z^2} \\ \tan^{-1}\left(\frac{y}{x}\right) \\ \sin^{-1}\left(\frac{z}{\sqrt{x^2+y^2+z^2}}\right) \end{bmatrix} + v. \tag{5}$$

With the inverse sensor model, the Cartesian coordinates can be derived from any measured sample:

$$\begin{bmatrix} x \\ y \\ z \end{bmatrix} = \boldsymbol{h}^{-1}(r,\alpha,\varepsilon) = \begin{bmatrix} r\cos\alpha\cos\varepsilon \\ r\sin\alpha\cos\varepsilon \\ r\sin\varepsilon \end{bmatrix}. \tag{6}$$

From a technical viewpoint, LiDARs are categorized into the following currently widespread types:

- Digital spinning LiDAR: emits electronically controlled laser beams, which produce fully structured vertical and horizontal data.
- Analog spinning LiDAR: timed beaming, vertically structured, but horizontally unstructured data.
- Raster-scanned LiDAR: raster scanning of the view angle field (similarly to cameras), unstructured horizontal and vertical data. Beam control is accomplished with MEMS mirror. The field of view can be varied in one axis.

The use of LiDARs in automotive settings imposes some harsh requirements for qualification, like water/dust/vibration protection and relatively low power consumption (~20 W). LiDARs on vehicles should also use laser beams that are not visible and do not damage human vision in any way (Laser class I).

2.3 Cameras and Stereo cameras

Cameras measure color pixels in the environment. From a technical side, current widespread camera sensors are based on CMOS and CCD technology.

Mathematically speaking and based on the fundamental results of optics, a camera remaps 3D color information into a 2D plane. Complex models take lens attributes into account. The simplest camera model (camera pinhole model, Fig. 2) does not use lens properties and can be used to describe basic image mapping. In this model, the measured point appears through a normalized plane

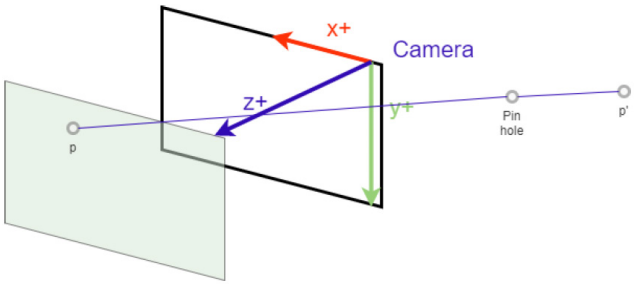

Fig. 2 Illustration of camera pinhole model

on the physical retina. In the internal frame of the camera, a slightly different coordinate system is used, with the origin point in the top-left corner of the retina plane. The x-y axes are defined on the retina plane, while the z-axis points outward the camera.

The main task is to map pixels from the world frame. A single pixel of the world can be mapped with the following relations:

$$\hat{\boldsymbol{p}}(\hat{x},\hat{y},1)^T \overset{def}{=} \begin{cases} \hat{x} = \dfrac{x}{z} \\ \hat{y} = \dfrac{y}{z} \end{cases} \Leftrightarrow \hat{p} = \frac{1}{z}[I\ 0]\,p. \tag{7}$$

As the pixels are not necessarily square but rectangular, linear scaling is required to get the final transformation for the $\hat{p}$ retinal point:

$$\boldsymbol{p}[x,y] = \begin{cases} x = kf\dfrac{x}{z} = kf\,\hat{x} \\ y = lf\dfrac{y}{z} = lf\,\hat{y} \end{cases}. \tag{8}$$

In the case of CCD cameras, the origin is not the corner of the image plane. Therefore an offset must be added to the pixels (using $\alpha = kf, \beta = lf$):

$$\boldsymbol{p}[x,y] = \begin{cases} x = \alpha\hat{x} + x_0 \\ y = \beta\hat{y} + y_0 \end{cases}. \tag{9}$$

If there is a slight slip in the coordinate system of θ angle (e.g., due to manufacturing error), Eq. (9) is modified as Eq. (10):

$$\boldsymbol{p}[x,y] = \begin{cases} x = \alpha\hat{x} - \alpha\cot\theta\,\hat{y} + x_0 \\ y = \dfrac{\beta}{\sin\theta}\hat{y} + y_0 \end{cases}. \tag{10}$$

Besides the image mapping model, cameras are attributed with intrinsic (e.g., focal length) and extrinsic parameters (i.e., the transformation between the camera and world frame).

In automotive scenarios, stereo cameras and multi-camera systems are increasingly popular. Multi-cameras perform the synchronized fusion of multiple camera images. Therefore single-camera image mapping can be based on simple camera model superpositions. The advantage of stereo cameras is that they can produce a depth map (and a point cloud using this depth map) based on the synchronized pictures. The most basic parameter is the baseline (distance between the two lenses). In computational models, it can be assumed that both cameras have precisely the same properties (e.g., f focal length). The stereo-camera conceptual model is depicted in Fig. 3.

Depth can be estimated using elementary geometry, using the measurement of the point from both cameras (x_r and x_l). Based on the theorem of similar triangles, and the disparity $d = x_l - x_r$:

$$\frac{T+d}{Z-f} = \frac{T}{Z} \Rightarrow Z = f\left(\frac{T}{d}\right). \tag{11}$$

This disparity can be used to generate depth information, similarly to the measurement of LiDARs.

2.4 Radar

The radar (radio locator) perceives objects using radio waves and echolocation. Radars can be used perfectly in automotive applications like adaptive cruise control or obstacle avoidance. Radars can operate in a wide range, typically between 2–300 meters. The following radars are widespread in vehicles with distinct operational background:

- *Pulse-Doppler radars* are of a wide range (few kilometers). Such radars transmit radio waves for a short period and switch to receiving mode to process echoed waves. Typical vehicular requirements demand fast computation, which requires high-speed analog circuitry, high digital sampling time,

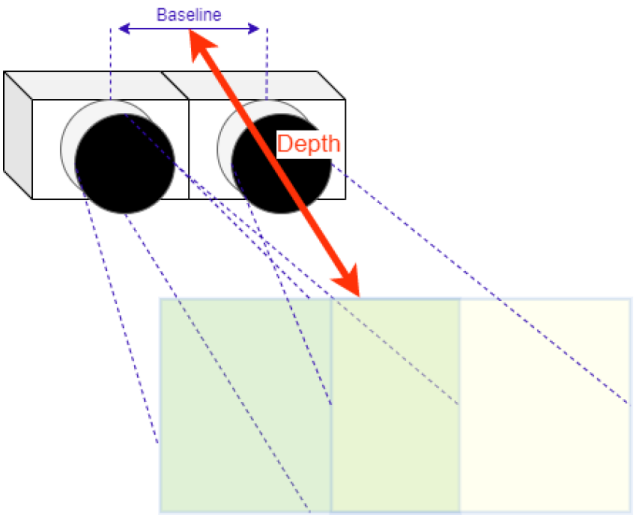

Fig. 3 Illustration of stereo camera model

and signal processing capabilities. This cannot be afforded in conventional vehicles.

- In conventional vehicles, *frequency-modulated continuous-wave* (FMCW) radars are used. They require less complex electronics and radio frequency circuitry to satisfy automotive requirements. This can be achieved by using FPGAs, special microprocessors, or special ASIC devices. Manufacturers like Continental AG produce this type in high volume at an affordable cost. This type of radar is described in more detail below.

FMCW radars use a continuous carrier frequency, which can be used to process information by analyzing its echolocation (Fig. 4). The frequency is cyclically variable. To ensure that the transmitting signal does not interfere with receiving side, separate transmitter and receiver antennae are used.

Range is estimated by measuring frequency difference. There is no amplitude modulation in this process. When the transmitter frequency increases, the receiver frequency will be slightly smaller, depending on time delay. When the receiver frequency decreases, this difference will be larger. The measured frequency differences will be proportional with the round-trip time (RTT), higher the measured distance, higher this delay is. Typical operational frequencies are 24 GHz and 77 GHz. These frequencies are typically used because of small antennae size, high availability of spectral range and attenuation of radio waves.

3 Calibration methods

Each sensor configuration requires two calibration tasks, *internal* and *external calibration*. *External calibration* can be viewed as a task of finding a mapping between the kinematic frame of the sensor and the primary reference frame of the vehicle (e.g., the center of the rear/front axle). The result of this process is independent of the sensor type itself. More formally, the whole process can be written as finding an optimal 6-DOF $\boldsymbol{T}^{X,S}$ the transformation between the main reference frame and the frame of the sensor:

$$\boldsymbol{T}^{X,S} = \begin{bmatrix} \boldsymbol{R} & \boldsymbol{t} \\ \boldsymbol{0}^T & \boldsymbol{1} \end{bmatrix}. \tag{12}$$

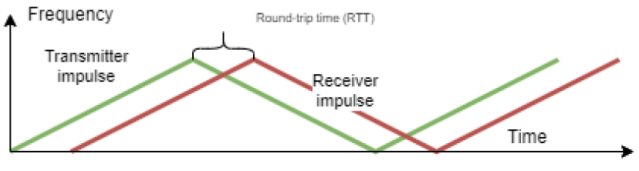

Fig. 4 FMCW signal operation

In this matrix, $\boldsymbol{R}$ is a 3D rotation, $\boldsymbol{t}$ is a 3D translation vector. The transformation can be parameterized with vector $\theta^{1,2} = (t_x, t_y, t_z, v_x \cdot \alpha, v_y \cdot \alpha, v_z \cdot \alpha)$, α rotation angle, and rotation axis (v_x, v_y, v_z). Finding this parameterization vector can be formalized as input for an optimization problem.

Internal calibration is highly dependent on the sensor itself. The result of internal calibration is a parameter set to configure the target sensor. Sensor producers usually provide configuration sets resulting from internal calibration. Consequently, developers can usually omit this step, especially in the prototype phase of the development.

On the other hand, external calibration depends heavily on the sensor placements, so it is performed on the target platform. In this article, we focus primarily on external calibration methods. In summary, the external calibration poses more challenges, and it can be done automatically in multi-sensor setups, where radar/LiDAR/camera are simultaneously operating.

3.1 Overview of feature matching

Feature matching algorithms are an essential building block of calibration methods. Feature matching is usually performed on point clouds natively produced by LiDARs (and in some cases multi-camera systems) and can be easily computed from stereo camera imagery.

The task is to find an optimal homogeneous transformation between the two (partial) point clouds during calibration. Popular approaches are *iterative closest point* (ICP) (Besl and McKay, 1992) or a more recent method called Normal Distribution Transform (NDT) (Biber and Straßer, 2003). Besides their use in sensor calibration, these approaches can be used in localization problems. Additional circumstances can be assumed during calibration. The ground can be considered as a nearly perfect plane, facilitating the plane matching process. The optimized version of all these algorithms are included in popular libraries like Point Cloud Library (PCL).

3.2 Optimization methods

As calibration outputs an optimal homogeneous transformation, various optimization methods are employed to find the best-matching transformation. The most convenient way is to use some variant of the gradient-based method. More complex methods use *genetic-algorithms* to perform this task. Both approaches are available in widespread developer environments. The calibration task is formulated as a graph optimization problem using other techniques (e.g., using G2O). This approach is useful in many-sensor

configurations, with different possibilities of transformation layouts. Due to the possible nonlinearity of the optimization problem, Levenberg-Marquadt (LM) or Semi-global Matching algorithm is used instead of Newton's method.

3.3 Camera calibration

The extrinsic and intrinsic calibration of cameras is well-known and has been integrated into popular computer vision frameworks (e.g. OpenCV, Bradski (2000)). During intrinsic camera calibration, the focal length and the distortion parameters are derived, which are mostly contributed by the equipped lens and camera sensors. Intrinsic calibration is carried out with a target checkboard table with known width, height, and uniform size of each cell. An example of this process is depicted in Fig. 5.

The camera model can be formalized as matrices, which can be decomposed into the internal and extrinsic parameters. Intrinsic parameters describe the camera properties (e.g. field of view, focal length), which can be used to calculate a point in the environment as an image plane pixel, by solving the matrix equation $\boldsymbol{p} = 1/z[\boldsymbol{K},0]\boldsymbol{p}_c$. Assuming no distortion and slip, this matrix is given as:

$$\boldsymbol{K} = \begin{bmatrix} kf & 0 & x_0 \\ 0 & lf & y_0 \\ 0 & 0 & 1 \end{bmatrix}. \tag{13}$$

The matrix $\boldsymbol{K}$ can be rewritten with assuming θ slip angles as:

$$\boldsymbol{K} = \begin{bmatrix} kf & -kf\cot\theta & x_0 \\ 0 & \dfrac{lf}{\sin\theta} & y_0 \\ 0 & 0 & 1 \end{bmatrix}. \tag{14}$$

External calibration provides the same extrinsic transformation, in the same way as in the case of other sensors.

Fig. 5 Example of camera calibration process with calibration table

As a reminder, this matrix is a homogeneous transformation:

$$\boldsymbol{P}_c = \begin{bmatrix} \boldsymbol{R} & \boldsymbol{t} \\ \boldsymbol{0}^T & \boldsymbol{1} \end{bmatrix} p_W. \tag{15}$$

Matrix $\boldsymbol{P}_c$ can be used to transform a point from the world reference frame to the camera reference frame. This can be used to define mapping using both matrices:

$$\boldsymbol{p} = \frac{1}{z}\boldsymbol{K}\begin{bmatrix}\boldsymbol{R} & \boldsymbol{t}\end{bmatrix}. \tag{16}$$

During calibration, the task is to find an optimal set of these matrices. In the case of cameras, there exists a matrix-decomposition based approach to find these matrices (e.g. using QR decomposition).

3.4 Camera calibration

The earliest multi-sensor calibration methods used camera and LiDAR for external calibration. In multi-sensor configurations, generally LiDAR is assumed as the main reference and other sensor output is matched to the LiDAR point cloud using an optimization method. This is due to the following properties of LiDAR data:

- In the case of LiDARs, internal calibration is almost always provided by the manufacturer, the internal parameters are usually set precisely enough.
- With the help of LiDARs, geometric properties can be easily measured, like in a static environment. This allows the easy registration of points measured by the camera in the LiDAR point cloud.

The different methods and the target sensors are summarized in Table 2. The listed methods are capable to calibrate external methods.

Similarly to single camera calibration, multi-sensor calibration requires a calibration table. Features on this calibration table are detectable both by a camera and LiDAR. An example of such table is depicted in Fig. 6. The four circular holes on Table 2 are easily detectable by both the LiDAR and camera. In other methods like in Rodriguez F. (2008), an ellipse is fitted on the measured point cloud.

Table 2 Comparison of multi-sensor calibration methods

Source	LiDAR	RADAR	Stereo	Mono
Guindel et al. (2017)	Y	N	Y	N
Sim et al. (2016)	Y	N	Suboptimal	Y
Dhall et al. (2017)	Y	N	Y	Y
Rodriguez F. et al. (2008)	Y	N	N	Y
Domhof et al. (2019)	Y	Y	Y	Y

Guindel et al. (2017) introduces a calibration method, which can be used to calibrate LiDAR-camera sensor configurations. The calibration table is the same as above (Fig. 6). An ROS-based implementation of this method is publicly available, with additional test data. Other calibration methods are inspired from this algorithm. This algorithm registers the stereo-camera measured points on the LiDAR point cloud. Based on the monochromatic picture from the stereo camera the depth points estimated by the registration algorithm are associated with each LiDAR point. The similarity between each point cloud results from the transformation between both sensors. The transformation optimization is based on SGM method. The algorithm performs the following steps:

1. Generating a representation from camera and LiDAR.
2. Search for discontinuities (planes) to find the calibration table in the point cloud. Exploiting the properties of the calibration table, the plane can be found with *sampling consensus-based* (SAC) method. RANSAC helps to separate walls and other environmental elements from the table. The geometric features on the calibration table can be found with conventional algorithms, like Sobel-filtering (intermediate process is illustrated in Fig. 7).
3. The calibration table contains four circles, which can be methodically detected in the point cloud. The precision can be further improved by filtering out outlier points.
4. In the final registration, a transformation parameter set is searched that minimizes the distance between the geometric centre of both point clouds. Rotation is not assumed in the initial step, which can be calculated by solving a system of 12 equations with least squares. This results in 3 final equations, which can be solved by QR decomposition. Finally, ICP finds a final transformation between the two point clouds.

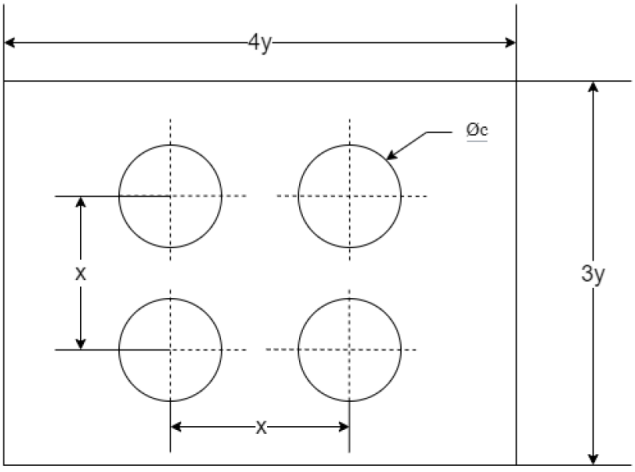

Fig. 6 An example of calibration table used in LiDAR-Camera calibration (with a rectangle side ratio of 3:4)

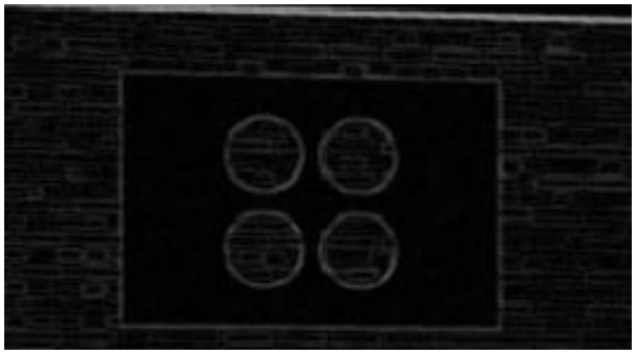

Fig. 7 Intermediate calibration step, Sobel-filtering to find geometric features using calibration method based on Guindel et al. (2017) in a simulated setup (reproduced Gazebo simulation output by the authors)

Dhall et al. (2017) presents an alternative method to calibrate LiDAR and camera configurations. This uses multiple calibration tables, with Aruco markers as camera detectable features (Fig. 8).

The point clouds and the measured Aruco marker centers are minimized with the help of iterative closest point, formally the following problem is solved on the extrinsic transformation:

$$\underset{R\in SO(3),\ t\in R^3}{argmin} \left\|(\boldsymbol{RP}+\boldsymbol{t})-\boldsymbol{Q}\right\|^2. \tag{17}$$

The iterative-closest point matches the closest point and finds an optimal $[\boldsymbol{R}|\boldsymbol{t}]$ transformation between the point clouds minimizing the Euclidean distance between the point clouds. To avoid degenerate cases, the Aruco marker corners are exploited to find a closed solution. Kabsch algorithm is used to find the rotation between the point clouds.

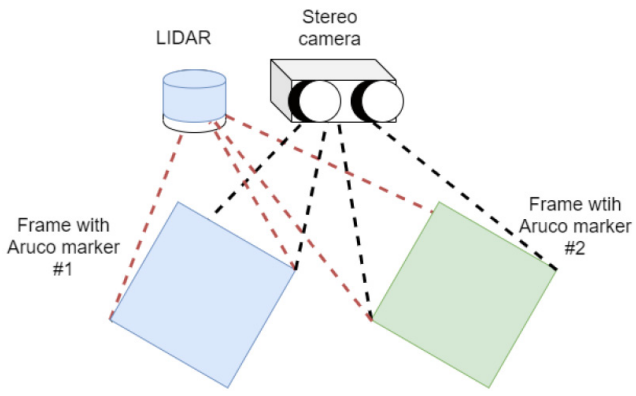

Fig. 8 Calibration layout proposed by (based on Dhall et al., 2017)

The motivation of this method is to calibrate multiple cameras that are not entirely in the same field of view. For the whole 360° field of view a LiDAR can be used for precise calibration.

3.5 Graph-based external calibration

A novel approach is presented by Domhof et al. (2019), which is potentially capable of calibrating arbitrary sensor configurations, including LiDARs, cameras, radars. It uses a calibration table similar to Rodriguez F. et al. (2008), extended with a tetrahedron on the back of the table detectable by the radar and conic holes (Fig. 9).

The external calibration can be formalized as follows: organize the sensors in an ordered list $\{1 \ldots K\}$, and measure the calibration table from K sensor locations. In the case of camera and LiDAR, these are 3D coordinates of each detected circle. The minimizable squared error of the external calibration is the Euclidean distance of the detected circles form sensor k:

$$\varepsilon_k\left(\theta^{1,2}\right)=\sum_{p=1}^{4}\left\|\boldsymbol{y}_{k(p)}^{2}-\boldsymbol{T}^{\mathbf{1,2}}\cdot\boldsymbol{y}_{\boldsymbol{k}(\boldsymbol{p})}^{\mathbf{2}}\right\|^{2}. \tag{18}$$

In the case of the radar, they are the planar coordinates of the tetrahedron on the back of the table. The minimizable error is the distance of the tetrahedron using the position of the detected circles:

$$\varepsilon_k\left(\theta^{1,R}\right)=\left\|\boldsymbol{y}_{k(1)}^{R}-\boldsymbol{p}\left(\boldsymbol{T}^{\mathbf{1,R}}\cdot\boldsymbol{g}\left(y_k^1\right)\right)\right\|^{2}. \tag{19}$$

These metrics allow the formalization of the optimization problem to find an optimal transformation, which minimizes the $f(\theta^{1,2})$ cumulative error of all K calibration measurements ($\boldsymbol{\mu}_k^2\cdot\boldsymbol{\mu}_k^1$ indicators ensure that only those detected by both sensors are taken into account):

$$f\left(\theta^{1,2}\right)=\sum_{k=1}^{K}\boldsymbol{\mu}_k^2\cdot\boldsymbol{\mu}_k^1\boldsymbol{\varepsilon}_k\left(\boldsymbol{\theta}^{\mathbf{1,2}}\right). \tag{20}$$

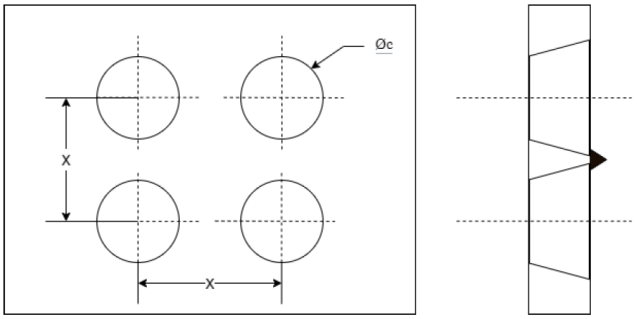

Fig. 9 Calibration table used by Domhof et al.© (2019), with the triangular component on the back of the frame for radar calibration

The exotic many-sensor configurations are most naturally depicted in a directed (acyclic) graph-based layout, with the main reference point as a special node in this graph. This algorithm offers three differently organized layout types (the layouts are depicted in Fig. 10).

In the case of minimally connected pose estimation (MCPE) layout, a sensor is selected as the primary reference sensor, and the other sensor transformations are relative to this special sensor. The edges are minimal in this layout. The optimization function, in this case, is the following:

$$f\left(\theta\right)=\sum_{i=2}^{N}\left[\sum_{k=1}^{K}\boldsymbol{\mu}_k^i\cdot\boldsymbol{\mu}_k^1\cdot\boldsymbol{\varepsilon}_k\left(\boldsymbol{\theta}^{1,i}\right)\right].$$

The fully connected pose estimation (FCPE) layout has been inspired by SLAM methods. All sensors are considered at once with a loop-closure constraint (formally $\left(\boldsymbol{T}^{s_l,1}\cdot\boldsymbol{T}^{s_{l-1},\ s_t}\cdot\ldots\cdot\boldsymbol{T}^{\mathbf{1,2}}\right)-l=0,\ \forall l\ s_l$ equals with the sensor count in the cycle) to ensure all cycles are equal with the identity matrix. This method calculates all $C(n, 2)$ transformation matrix combinations instead of the $N-1$ transformation matrices, by considering the following total error function:

$$f\left(\theta\right)=\sum_{i=1}^{N}\sum_{j=i+1}^{N}\left[\sum_{k=1}^{K}\boldsymbol{\mu}_{\boldsymbol{ki}}\cdot\boldsymbol{\mu}_{\boldsymbol{k}}^{\boldsymbol{j}}\boldsymbol{\varepsilon}_k\left(\boldsymbol{\theta}^{\boldsymbol{i,j}}\right)\right]. \tag{21}$$

Adding additional error factors possibly ensures robustness to noise instead of using only one reference sensor. On the other hand, error factors increase in a quadratic proportion of the sensor count, and additional loop closure constraints must be added.

Pose and structure estimation (PSE) layout optimizes the transformations based on an explicit estimation. In this layout, the task is to estimate the structure of the poses $M = (m_1, \ldots, m_k)$ and the $\boldsymbol{T}^{\boldsymbol{M,i}}$ transformation in a fixed reference frame for all i sensors. The estimations are $\hat{\boldsymbol{y}}_{k(p)}^{M}\boldsymbol{h}\left(m_k,\ p\right)$ samples that follow a standard Normal distribution with zero mean-value (each estimation can be derived as $\boldsymbol{y}_{k(p)}^{i}=\boldsymbol{T}^{M,i}\cdot\hat{\boldsymbol{y}}_{k(p)}^{M}+\eta^{i},\ \eta\sim N\left(0,\Sigma^{i}\right)$). Instead

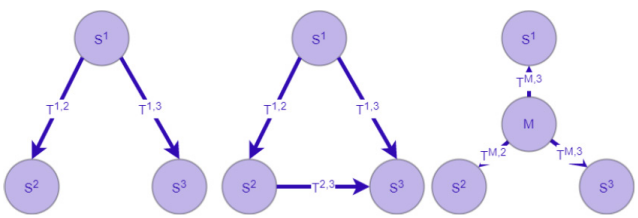

Fig. 10 Different graph-based layouts of sensor calibrations (left-to-right): MCPE, FCPE, PSE

of Euclidean distance, Mahalanobis-distance can be used. In the initial step, all Σ^i matrices are equal to the identity matrix, and the transformation is optimized per kinematic joint:

$$\varepsilon_k\left(\theta^{M,i}, \boldsymbol{M}\right) = \sum_{p=1}^{4} \boldsymbol{D}^2_{\Sigma^i}\left(\hat{\boldsymbol{y}}^i_{k(p)},\ \boldsymbol{T}^{M,i} \cdot \boldsymbol{y}^M_{k(p)}\right), \tag{22}$$

$$f\left(\theta, \boldsymbol{M}\right) = \sum_{i=1}^{N}\left[\sum_{k=1}^{K} \boldsymbol{\mu}^i_k \cdot \boldsymbol{\varepsilon}_k\left(\theta^{M,i}, \boldsymbol{M}\right)\right]. \tag{23}$$

Intermediate results can be used to re-estimate the noise covariances and to re-evaluate $f(\theta, \boldsymbol{M})$. This step can be repeated until the convergence of all variances. In this case, $\boldsymbol{T}^{M,i}$ must be fixed to avoid non-unique solutions. The downside of this layout that the error function is a homogeneous estimation which can be defined as negative log-likelihood. The combination of these squared functions leads to heterogeneous error (pixel vs. Euclidean error). The optimization is complex compared to other layouts. Consequently, the loop closure is not explicitly constrained. On the other hand, the probabilistic formalization allows easy injection of a priori data of the calibration table and the sensor poses.

The graph-based layout allows the result to be stored in a graph-based format. Such format is the unified robot description format (URDF), which is widespread in robotic applications. This algorithm is publicly available at a GitHub repository maintained by the author of the article (EaiPool, 2021).

4 ADAS Sensor calibration and diagnostics laboratory

The calibration and preferably automatic calibration of automotive sensors has became a priority nowadays. This demand is contributed to the increasing appearance of autonomous vehicles and the growing sensory capabilities of conventional vehicles. While the extensive use of sensors in autonomous vehicles is obvious, conventional vehicles are also equipped with intelligent driver assistant features like adaptive cruise control and night vision. Fine-tuning, even mathematical investigation of these systems is reasonable, like in the work described by Derbel et al. (2012). To satisfy the increasing requirements both from academia and industry, numerous institutions started to install a (semi-)automatic calibration laboratory, like demonstrated by Varga et al. (2020).

The Department of Road and Rail Vehicles Diagnostics laboratory of Széchenyi István University at ZalaZone automotive proving ground is planning to install an ADAS calibration system for R&D and demonstrative purposes. The calibration setup has been purchased from Texa ADAS systems offering a calibration system (Radar and Camera Calibration System 2 - RCCS 2) suitable for most automotive sensor calibration tasks. Additionally, an ACS (All Around Calibration System) was / is planned to be purchased to perform a 360° camera system and rear & side sensor calibration. Both systems are also bundled with its calibration software, IDC5. The planned placement of the device and the proposed layout of the laboratory are depicted in Fig. 11.

On this designed layout, the placement of the vehicle is marked within specially designed areas for different types of measurements. The laboratory shall be equipped with the RCCS 2 and ACS systems that use the same frame holder for both sensor calibration processes, enabling both camera and radar sensor calibration. Furthermore, with the usage of one of the methods described in Section 3, joint extrinsic calibration of multiple sensors equipped on the vehicle could be likely carried out.

4.1 Calibration and diagnostic operations

In Section 4.1.1, the required preparations, and operations for sensor calibration with RCCS 2 are further discussed. As previously mentioned, RCCS 2 uses the same frame holder stand to carry out the camera and radar calibration.

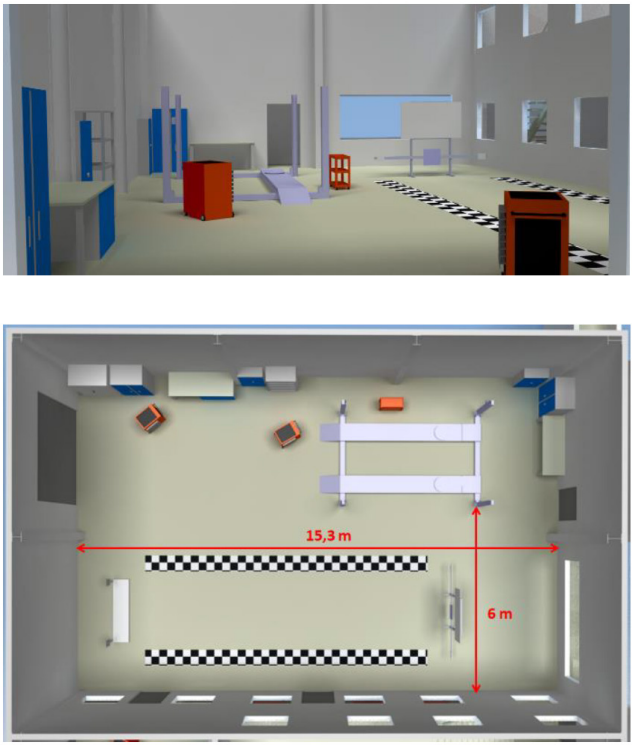

Fig. 11 Texa ADAS calibration placement (ZalaZone planned layout) (equiiped with devices from Texa Group)

The calibration process can be carried out without changing the vehicle position relative to the frame stand. RCCS 2 provides a laser telemeter to measure the vehicle's position for the precise positioning. RCCS 2 also provides the necessary tools to fix the vehicle into a stationary position (i.e., wheel lock). The exact requirements for the correct positioning are the following:

- The vehicle and the calibration unit must be coplanar (at 0° degrees to each other)
- The vehicle must be empty (boot and passenger compartment), meaning no person can be inside the vehicle.
- The steering wheel must be in a central position, and the wheels must be straight.
- The specific manufacturer recommendations must be satisfied on the target vehicle. Such requirements include proper oil level, tire pressure, coolant level, vehicle's wheel alignment. Also, the vehicle's front and the surroundings of the front radar sensor must be free.

RCCS 2 systems are also capable of integrated ground clearance measurement for more automatization of the overall calibration process.

4.1.1 Camera calibration

Using RCCS 2, the camera system can be calibrated using different camera calibration panels designed to operate on other electronic driver assistance systems (e.g., Night Vision System, Adaptive Cruise Control). The bundled software provides meaningful help to set the vehicle into the correct position for calibration. The following technological criteria must be met for proper calibration of the camera system:

- During camera calibration, the light reflexive objects and devices should not be placed on the grey lane.
- The wall color should be matte white with no reflection.
- In the grey lane, all objects of black color should be avoided.
- The wall should not contain any kind of texture, figure, or poster.
- If there is a window in front of the target camera, a white strip curtain should be used.
- There should be no person in the field of view of the target camera (except when human movement simulation is part of the calibration process like in the case of BMW vehicles).
- The grey area must be illuminated adequately; the stand should not cast a shadow on the wall behind it.
- A lighting system of adjustable brightness or a layout divided into switchable segments should be used. In general, in most vehicle types, an adequately illuminated area is required, but medium brightness is more appropriate in some vehicles.

The camera calibration process of the vehicular camera in the case of the Texa ADAS RCCS Calibration System 2 device and the installed frame is depicted in Fig. 12.

4.1.2 Radar calibration

The radar system can be calibrated with the RCCS frame holder stand (the process is illustrated in Fig. 13). Here are some preliminary technical notes regarding the calibration process:

- Using the RCCS stand, there is no special lighting requirement of radar calibration so that the calibration can be executed in inadequate lighting conditions (i.e., in the dark).

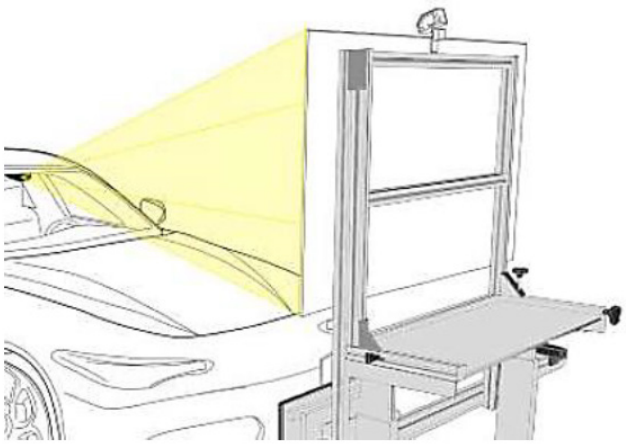

Fig. 12 Camera calibration with the Texa ADAS RCCS Calibration System 2

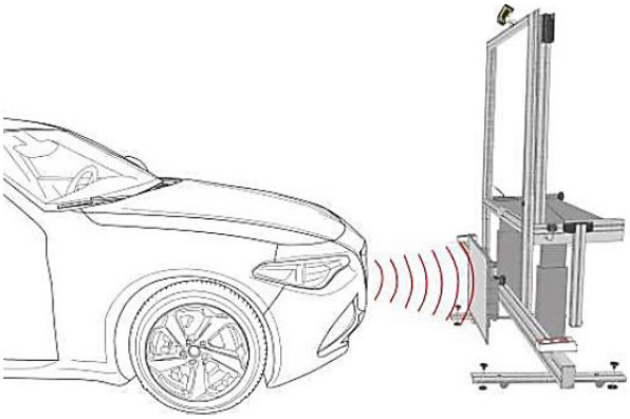

Fig. 13 Radar calibration with RCCS 2 (no personnel, metal objects, antennas or radio transmitters of any kind are allowed in the grey area)

- Between the radar calibration plate and the vehicle, all metallic objects should be avoided.
- Japanese vehicles (e.g., Honda, Toyota, Mazda) can be calibrated using a radar-wave reflection cone.

4.1.3 360° sensory system calibration

It is also possible with the proposed laboratory setup and equipment to calibrate 360° camera and radar systems. In the case of 360° (full surround) systems, the required space for the proper placement of the calibration device is depicted in Fig. 14. This calibration is performed with ACS system instances installed around the car (inside the checkerboard pattern lanes of the laboratory layout). The calibration frames are of similar composition as in single-sensor setups but are slightly different. As automotive sensors on the side and the rear have a deeper placement with a different field of view than the front sensors, ACS frame stands are constructed differently. Calibration frames are placed on the side points of the aluminum stand. This enables the calibration of sensors placed in different positions of the vehicle. The perpendicular placement of the calibration stand can be maintained with the markings of the laboratory layout.

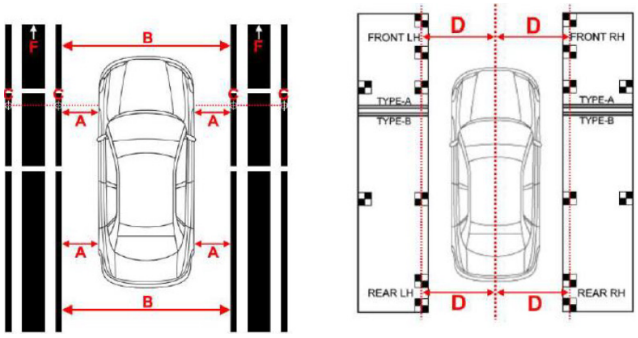

Fig. 14 Calibration area in the case of 360° sensor systems (B = 2000–2500 mm), and the respective reference marks

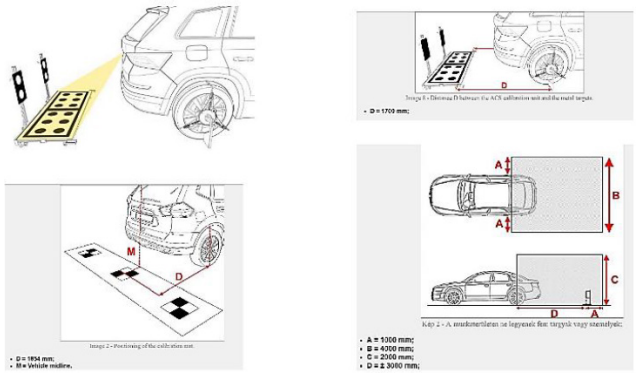

Fig. 15 Placement of the calibration mat, dead-angle and rear-side radar calibration

Calibration of side and rear sensors

Using the ACS calibration frame, the rear and side sensors can be calibrated with the calibration frame (Fig. 15). In the case of rear sensor calibration, a calibration mat is additionally placed for precise measurements and for the estimation of the dead angle of the rear sensors.

5 Further work

After the installation of calibration devices and the equipment of the laboratories, numerous research directions are planned. A particular research field is related to traffic safety connections, where different themes can be designated:

1. Repairing of vehicles damaged in accidents.
2. Calibration operations after windshield replacement.
3. Evaluation of traffic safety effects posed by incorrectly calibrated sensors.

An important area during the calibration process is the validation of models based on measurement data. Once the the laboratory is equipped, the collection of empirical data and measurements of academic purpose will be of high focus.

6 Conclusions

This paper presented a laboratory for the automotive calibration processes. The laboratory equipment has been presented, capable of the sensory calibration of both conventional vehicles and autonomous vehicles. The calibration focuses on radar and camera calibration, as conventional vehicles are more frequently equipped with these sensor types. The purchased equipment can carry out frontal sensor (camera and radar), 360° system, and side-rear calibration. The equipment includes calibration frames (for different use-cases, e.g., night vision, ACC), digital equipment, and stands. The laboratory and its capabilities will be available shortly.

The recent relevant literature has been reviewed to enable the external calibration of autonomous vehicles. The internal calibration of individual sensors must be done precisely to ensure correct operation, just as in conventional vehicles. External calibration is additionally required to construct a kinematic tree of the sensory structure of the target vehicle. This kinematic tree is mandatory to operate algorithms used in motion planning, perception, and localization. The reviewed papers provide methods capable of the joint external calibration of multiple sensors.

In summary, the algorithms based on the reviewed material and the proposed laboratory equipment will provide a way to carry out all tasks required to perform precise and reliable calibration of the modern vehicle sensory systems.

Acknowledgement

The research presented in this paper was funded by the "Thematic Excellence Program – Institutional Excellence Subprogram – Digital Industrial Technologies Research at Széchenyi István University (TKP2020-IKA-10)" project.

References

Besl, P. J., McKay, N. D. (1992) "A method for registration of 3-D shapes", IEEE Transactions on Pattern Analysis and Machine Intelligence, 14(2), pp. 239–256. https://doi.org/10.1109/34.121791

Biber, P., Straßer, W. (2003) "The Normal Distributions Transform: A New Approach to Laser Scan Matching", In: Proceedings 2003 IEEE/RSJ International Conference on Intelligent Robots and Systems (IROS 2003) (Cat. No.03CH37453), Las Vegas, NV, USA, pp. 2743–2748. ISBN 0-7803-7860-1 https://doi.org/10.1109/IROS.2003.1249285

Bradski, G. (2000) "The OpenCV Library. Dr. Dobb's Journal of Software Tools, (4.7.0)", [computer program] Available at: https://opencv.org [Accessed: 04 April 2023]

Derbel, O., Péter, T., Zebiri, H., Mourllion, B., Basset, M. (2012) "Modified Intelligent Driver Model", Periodica Polytechnica Transportation Engineering, 40(2), pp. 53–60. https://doi.org/10.3311/pp.tr.2012-2.02

Dhall, A., Chelani, K., Radhakrishnan, V., Krishna, K. M. (2017) "LiDAR-Camera Calibration using 3D-3D Point correspondences", [preprint] arXiv, arXiv:1705.09785, 27 May 2017. https://doi.org/10.48550/arXiv.1705.09785

Domhof, J., Kooij, J. F. P., Gavrila, D. M. (2019) "An Extrinsic Calibration Tool for Radar, Camera and Lidar, In: 2019 International Conference on Robotics and Automation (ICRA), Montreal, QC, Canada, pp. 8107–8113. ISBN 978-1-5386-8176-3 https://doi.org/10.1109/ICRA.2019.8794186

EaiPool (2021) "Multi_Sensor_Calibration", [computer program] Available at: https://github.com/tudelft-iv/multi_sensor_calibration [Accessed: 04 April 2023]

Guindel, C., Beltrán, J., Martin, D., García, F. (2017) "Automatic Extrinsic Calibration for Lidar-Stereo Vehicle Sensor Setups", In: 2017 IEEE 20th International Conference on Intelligent Transportation Systems (ITSC), Yokohama, Japan, pp. 1–6. ISBN 978-1-5386-1527-0 https://doi.org/10.1109/ITSC.2017.8317829

IEEE Standards Association (2019) "1588-2019 IEEE Standard for a Precision Clock Synchronization Protocol for Networked Measurement and Control Systems", IEEE Standards Association, Piscataway, NJ, USA. https://doi.org/10.1109/IEEESTD.2020.9120376

Rodriguez F., S. A., Fremont, V., Bonnifait, P. (2008) "Extrinsic calibration between a multi-layer lidar and a camera", In: 2008 IEEE International Conference on Multisensor Fusion and Integration for Intelligent Systems, Seoul, South Korea, pp. 214–219. ISBN 978-1-4244-2143-5 https://doi.org/10.1109/MFI.2008.4648067

Sim, S., Sock, J., Kwak, K. (2016) "Indirect Correspondence-Based Robust Extrinsic Calibration of LiDAR and Camera", Sensors, 16(6), 933. https://doi.org/10.3390/s16060933

Texa Group "ADAS RCCS Calibration System 2: ADAS - Advanced Driver Assistance Systems – Texa S.p.a", [computer program] Available at: https://www.texa.com/products/adas-radar-camera-calibration-kit/ [Accessed at 10 April 2023]

Texa Group "TEXA", [online] Available at: https://www.texa.com/ [Accessed: 04 April 2023]

Varga, B., Szalai, M., Fehér, Á., Aradi, S., Tettamanti, T. (2020) "Mixed-reality Automotive Testing with SENSORIS", Periodica Polytechnica Transportation Engineering, 48(4), pp. 357–362. https://doi.org/10.3311/PPtr.15851